nature catalysis

Article

https://doi.org/10.1038/s41929-023-00923-6

Electrocatalytic dual hydrogenation of organic substrates with a Faradaic efficiency approaching 200%

Received: 19 August 2022

Accepted: 18 January 2023

Published online: 20 February 2023

Check for updates

Guanqun Han, Guodong Li & Yujie Sun

The wide deployment of electrocatalytic hydrogenation may be hindered by intrinsic limitations, including substrate solubility and difficult separation of the products from the electrolyte. The use of palladium membrane electrodes can overcome the aforementioned limitations by physically separating the formation of reactive hydrogen atoms from the hydrogenation of unsaturated organic substrates. Here, by taking advantage of the low-potential oxidation of formaldehyde on a palladium membrane anode to produce hydrogen that can permeate through the membrane electrode, we demonstrate that electrocatalytic dual hydrogenation of unsaturated dicarboxylic acids is possible when another palladium membrane electrode is also adopted as the cathode. Such a design enables the electrocatalytic hydrogenation of the same substrate at both the anode and cathode in two separated chambers spatially isolated from the electrochemical cell with a theoretical maximum Faradaic efficiency of 200%.

Hydrogenation plays an important role in the chemical industry because nearly 25% of all chemical processes, ranging from petroleum refining and chemical feedstock manufacturing to pharmaceutical synthesis, consist of at least one hydrogenation step[1,2]. Currently, thermocatalytic hydrogenation is the dominant strategy, which is typically conducted at high pressure and elevated temperature using molecular hydrogen (H_2) as both the reductant and hydrogen source[3–7]. The energy-intensive nature of thermocatalytic hydrogenation calls for the development of lower-cost and greener strategies. Against this backdrop, electrocatalytic hydrogenation is regarded as an appealing alternative[8–10] and indeed has been investigated since the beginning of the last century[11]. The primary advantage of electrocatalytic hydrogenation is that it can be driven by renewable electricity under ambient conditions and use water as the hydrogen source.

Electrocatalytic hydrogenation typically involves the generation of adsorbed hydrogen (H*) on the cathode, which then hydrogenates unsaturated substrates (Fig. 1a)[12]. In this case, an oxidation reaction simultaneously takes place at the counter electrode (that is, the anode), which may yield a low-value product (for example, O_2) and pay a large overpotential penalty due to its sluggish kinetics. Consequently, a considerable amount of attention has recently been devoted to exploring paired electrosynthesis, which enables the formation of two value-added products at both the cathode and anode[13–15]. Nevertheless, the market-size mismatch in the hydrogenation and oxidation products may lead to concerns regarding its large-scale deployment. An additional challenge is to ensure that the electrochemical conditions are suitable for both reductive and oxidative transformations. Furthermore, only protic electrolytes can be used to generate H*, which can limit substrate solubility and scope, while the addition of co-solvents likely results in an increase in resistance and hence the need for a high voltage. Finally, the downstream separation of products from the electrolyte should not be neglected and in some cases substantial energy input is demanded[16].

With these considerations in mind, we reasoned that it would be economically attractive to develop an electrocatalytic dual hydrogenation strategy that enables the hydrogenation of the same organic substrate if active H* could be generated on both the cathode and anode. Furthermore, it would be even better if these hydrogenation steps were to take place in two separated chambers spatially isolated from the electrochemical reactor, thereby avoiding the later troublesome separation of products from the electrolyte. Because of their unique and efficient hydrogen absorption ability, Pd membrane electrodes

Department of Chemistry, University of Cincinnati, Cincinnati, OH, USA. e-mail: yujie.sun@uc.edu

https://doi.org/10.1038/s41929-023-00923-6

were used to carry out hydrogenation in a chamber physically separated from the electrochemical cell nearly two decades ago[17–19]. It was reported that the H* generated from proton reduction on a Pd membrane cathode can permeate through the membrane electrode to another compartment where hydrogenation occurs (Fig. 1b). Following the same strategy, more recently, Berlinguette et al. systematically investigated hydrogenation reactions in separated chemical chambers using Pd membrane reactors[20,21]. Besides cathodic hydrogenation, another oxidative transformation (for example, O_2 evolution or paired organic oxidation) proceeded on the anode (for example, Pt) and the overall voltage input of this type of electrolyser was usually larger than 1.5 V. Even though Pd electrodes have long been known for their hydrogen absorption and permeation capability[22], it has never been reported that such hydrogen permeation is feasible in Pd when used as an anode, probably because Pd is also a well-known electrocatalyst of the hydrogen oxidation reaction (HOR)[23].

It is also known that Pd is electrocatalytically active in the oxidation of formaldehyde following either a one-electron transfer (equation (1)) or a two-electron transfer (equation (2)) process[24].

$$HCHO + 2OH^- \rightarrow HCOO^- + 1/2H_2 + H_2O + e^- \quad (1)$$

$$HCHO + 3OH^- \rightarrow HCOO^- + 2H_2O + 2e^- \quad (2)$$

We reasoned that, according to the one-electron transfer process, if the anode-generated H* can permeate the Pd membrane anode to another chamber that is not in contact with the electrolyte, then the HOR could be avoided and instead hydrogenation in the outside chamber might be feasible. Here we report that the low-potential oxidation of formaldehyde to formate on Pd under alkaline conditions generates H*, which can indeed diffuse through the Pd membrane anode to drive hydrogenation reactions on the other side in a chamber spatially separated from the electrochemical cell. Furthermore, as shown in Fig. 1c, when two Pd membrane electrodes serve as the anode and cathode, with formaldehyde and water acting as the proton sources in the anolyte and catholyte, respectively, a four-compartment assembly is able to realize electrocatalytic dual hydrogenation of the same organic substrate in chambers outside of the electrochemical cell, with a theoretical maximum Faradaic efficiency of 200% (that is, one passed electron leads to two H* species). Finally, because of the favourable thermodynamic potential of formaldehyde oxidation to formate following the one-electron transfer process in alkaline electrolytes ($E = -0.22$ V versus the reversible hydrogen electrode (RHE))[25,26], we found the onset voltage input of this four-compartment assembly to drive the dual hydrogenation of maleic anhydride to produce succinic acid, a valuable chemical feedstock, to be as low as 0.4 V.

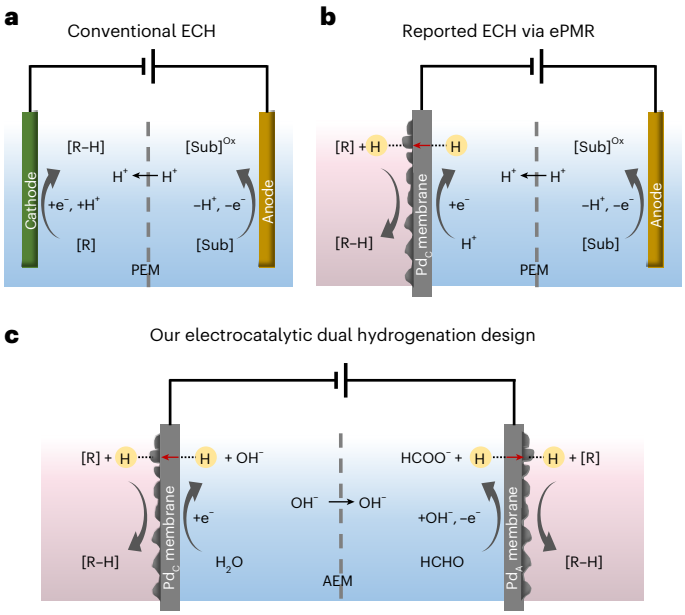

Fig. 1 | Schematics of three different electrocatalytic hydrogenation designs. **a**, Conventional electrocatalytic hydrogenation (ECH) at the cathode coupled with water or organic oxidation at the anode. **b**, Electrocatalytic hydrogenation on the other side of a Pd membrane cathode coupled with water or organic oxidation at the anode in an electrochemical palladium membrane reactor (ePMR). **c**, The proposed electrocatalytic dual hydrogenation strategy involves the use of a four-compartment assembly with two Pd membrane electrodes to enable hydrogenation to take place in two chemical chambers spatially separated from the electrochemical cell in which formaldehyde oxidation takes place at the anode with the generation of permeable hydrogen. Sub, substrate; Ox, oxidized; Pd_A, Pd anode; Pd_C, Pd cathode; PEM, proton exchange membrane; AEM, anion exchange membrane.

Results

Electrocatalytic dual H_2 production

As a commodity chemical, formaldehyde has a variety of industrial and medical applications and is also viewed as a liquid organic hydrogen storage compound[27,28]. A number of thermocatalytic systems have been reported to facilitate its partial or complete dehydrogenation to release H_2 under various conditions[28]. In alkaline electrolytes, a few electrodes (for example, Pd, Pt, Au, Cu and Ag) have been demonstrated to exhibit electrocatalytic formaldehyde oxidation properties[24,29,30]. As shown in Fig. 2a, when a commercial Pd foil (Alfa Aesar) was used as the anode, a rapid positive current rise was observed in 1.0 M KOH upon the addition of 0.6 M HCHO when the scanning potential was more positive than 0.25 V versus RHE. Further positive scanning resulted in the observation of gas bubbles emerging on the Pd surface. Supplementary Fig. 1 shows that the observed anodic current was highly dependent on the concentration of HCHO, with 0.6 M HCHO producing the highest current density of ~28 mA cm^{-2} at 0.5 V versus RHE; further increasing the HCHO concentration led to a decrease in the anodic current, likely due to the disproportionation of HCHO at high concentration in alkaline media (that is, the Cannizzaro reaction)[31]. To assess the impact of the disproportionation products on the oxidation of HCHO, chronoamperometry experiments were conducted with the sequential addition of 0.6 M HCHO followed by 0.1 M HCOOH or 0.1 M CH_3OH. As shown in Supplementary Fig. 2a, in the absence of HCHO, an extremely small capacitance current was observed. Upon the addition of 0.6 M HCHO, an immediate current rise was observed due to HCHO oxidation. After the introduction of 0.1 M HCOOH, a small but apparent current drop was observed, which was likely due to the competing adsorption of formate anions on the Pd anode, leading to fewer active sites available for HCHO oxidation. In contrast, as shown in Supplementary Fig. 2b, the addition of CH_3OH did not result in any change in the observed current, suggesting that CH_3OH could not be oxidized on Pd at this applied voltage and did not suppress the oxidation of HCHO either. Furthermore, increasing the hydroxide concentration from 0.1 to 1.0 M led to a steady rise in the anodic current when the electrolyte ionic strength remained constant (Supplementary Fig. 3). Finally, the cation effect of the supporting electrolyte was also probed: K^+ exhibited the highest anodic current followed by Na^+, Cs^+ and Li^+ (Supplementary Fig. 4). Consequently, 1.0 M KOH was used as the supporting electrolyte for all the subsequent experiments unless noted otherwise.

With the aim of developing a dual hydrogenation assembly, we also collected the linear sweep voltammogram (LSV) of a commercial Pd foil as a cathode in 1.0 M KOH. The LSV curve (purple curve) in Fig. 2a was obtained after several cathodic scans between 0 and −0.6 V versus RHE until the Pd foil was saturated with absorbed hydrogen. It was apparent that Pd was active towards water reduction and a current density of over 50 mA cm^{-2} could be reached within −0.5 V versus

https://doi.org/10.1038/s41929-023-00923-6

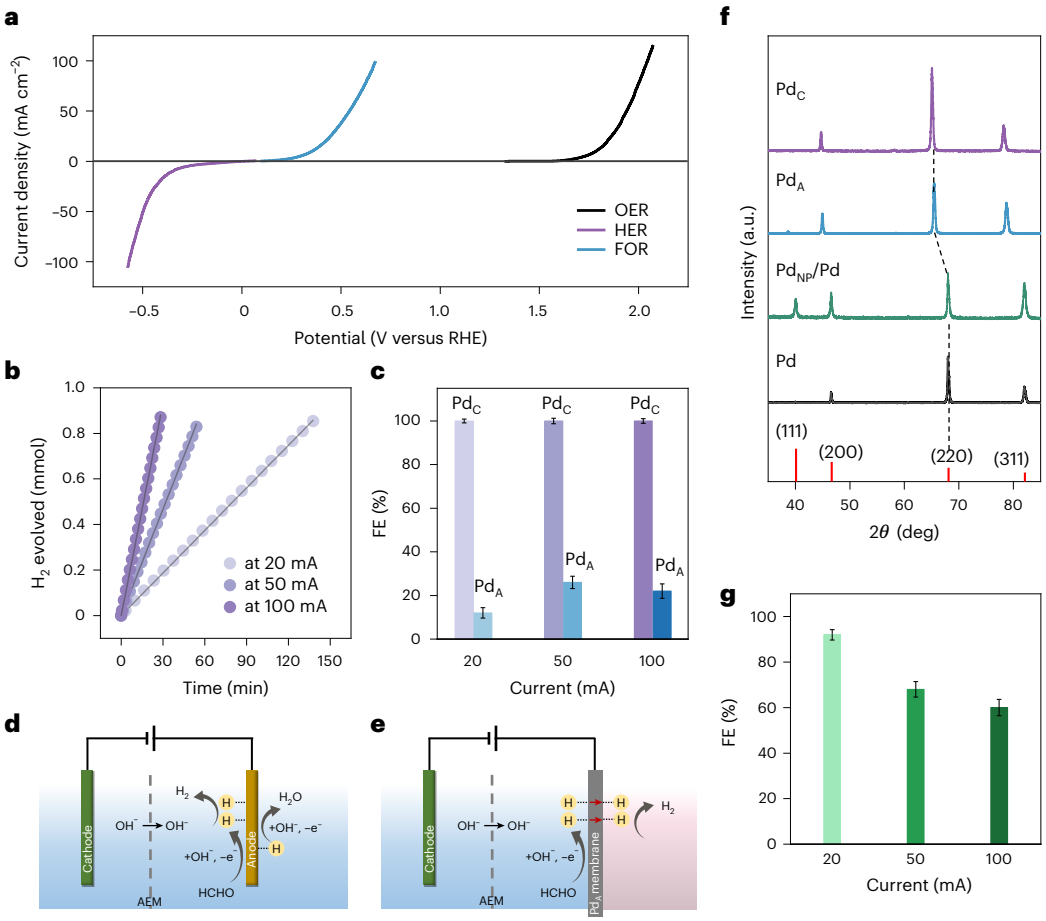

Fig. 2 | Comparison of electrocatalytic H_2 production and absorption using Pd electrodes. a, LSVs of a blank Pd foil as the anode in 1.0 M KOH in the absence (OER) and presence (FOR) of 0.6 M HCHO, and the LSV of a H-saturated Pd foil as the cathode in 1.0 M KOH (HER) using an H-cell in a three-electrode configuration. **b**, Profiles of electrocatalytic H_2 production on a Pd foil cathode during electrocatalysis performed at applied currents of 20, 50 and 100 mA. **c**, Faradaic efficiencies of H_2 production on Pd foils acting as the cathode and anode in an H-cell with a two-electrode configuration after passing 400 C charge of electrolysis at applied currents of 20, 50 and 100 mA. **d**, Schematic of the partial oxidation of HCHO followed by the HOR on a Pd anode immersed in the electrolyte. **e**, Schematic of the new design consisting of a Pd membrane anode through which the generated H* can permeate to form H_2 on the other side of the electrode. **f**, Powder XRD patterns of pristine Pd, electrodeposited Pd nanoparticles on pristine Pd foil (Pd_{NP}/Pd), a Pd anode and Pd cathode after passing 400 C charge of electrolysis at 50 mA, and the standard pattern of the face-centred cubic phase crystal structure of Pd (bottom). **g**, Faradaic efficiency of H_2 production on a Pd_{NP}/Pd membrane anode after passing 400 C charge of electrolysis at 20, 50 and 100 mA. The error bars indicate the standard deviations from measurements performed in triplicate. OER, oxygen evolution reaction; HER, hydrogen evolution reaction; FOR, formaldehyde oxidation reaction.

RHE. When this H-saturated Pd foil was used as the cathode for water reduction electrolysis, linear H_2 evolution was detected over the entire course of the electrolysis conducted at constant currents of 20, 50 and 100 mA (Fig. 2b); all matched the theoretical amounts of H_2 production derived from the passed charge very well. These results confirmed a Faradaic efficiency (FE) of 100% for the H_2 evolution reaction (HER) on a Pd cathode. In contrast, when the same Pd foil was used as an anode in the chronopotentiometry experiments of HCHO (0.6 M) oxidation in 1.0 M KOH at applied currents of 20, 50 and 100 mA, even though H_2 was indeed detected by gas chromatography (Supplementary Fig. 5), the amounts of H_2 produced were far less than the theoretical values based on passed charge. As shown in Fig. 2c, the calculated FEs of H_2 production were all less than 30% on a Pd anode. Such a drastic difference in H_2 production efficiency implies that effective hydrogen oxidation ($H^* \rightarrow H^+ + e^-$) occurs on Pd when it acts as an anode, which is in agreement with Pd being an active HOR electrocatalyst[23]. No CO_2 was detected in the anodic chamber, indicating that HCHO was not completely oxidized to CO_2 under these conditions. Because the Pd foil as anode was completely immersed in the electrolyte (Fig. 2d), the HOR was inevitable. However, this is not necessarily the case if a Pd membrane is used as the anode, when the other side of the membrane is not in contact with the electrolyte solution. As shown in Fig. 2e, this new design using a Pd membrane anode might provide an escape route for the H* generated from HCHO oxidation on the electrochemical side of the Pd membrane if hydrogen absorption into and diffusion through the bulk Pd membrane is possible. The realization of this hypothesis will enable H_2 evolution and hydrogenation in an adjacent chemical chamber that is spatially separated from the electrochemical cell by a Pd membrane anode.

As it is well documented that the crystalline lattice of Pd will expand following the absorption of hydrogen atoms[32], we collected the powder X-ray diffraction (XRD) patterns of Pd foils used as cathode and anode in the electrolytic partial oxidation of HCHO for comparison with that of a pristine Pd foil (Fig. 2f). The pristine Pd foil presents characteristic XRD peaks at 40.1, 46.5, 68.0 and 82.0°, corresponding to the (111), (200), (220) and (311) facets of its face-centred cubic (fcc) phase crystal structure (JCPDS card no. 46-1043), respectively. The lattice parameter of the pristine Pd foil was calculated to be 3.895 Å (ref. [33]), closely matching the literature value of 3.889 Å (ref. [34]). As expected, the XRD peaks of the post-electrolysis Pd cathode were shifted to smaller angles, as a

https://doi.org/10.1038/s41929-023-00923-6

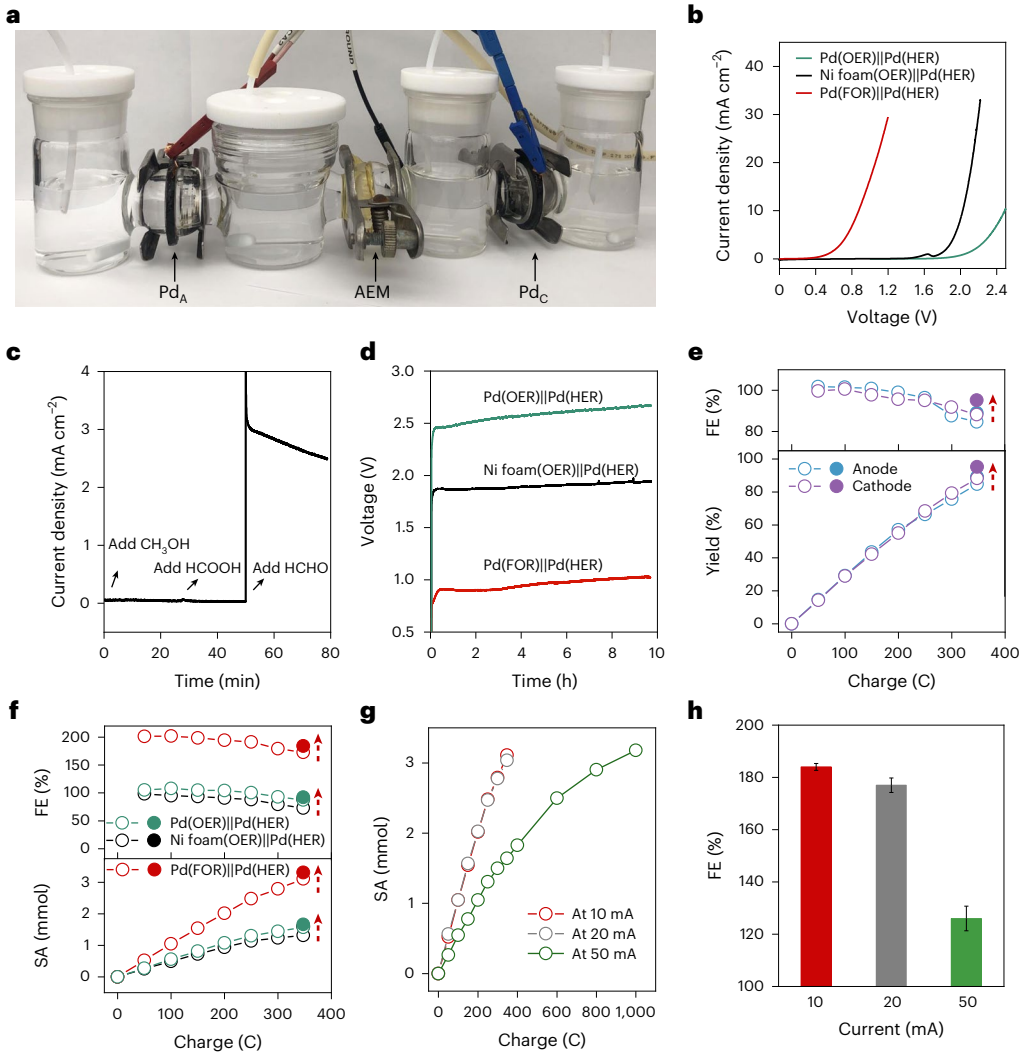

Fig. 3 | Electrocatalytic dual hydrogenation of maleic acid. a, A four-compartment assembly for electrocatalytic dual hydrogenation using Pd membrane electrodes as both the cathode and anode. **b**, LSVs obtained from the above four-compartment assembly in the absence and presence of 0.6 M HCHO in the anolyte and from a three-compartment assembly using a Pd_{NP}/Pd membrane cathode and a Ni foam anode (Supplementary Fig. 12). **c**, Chronoamperometry curve obtained from the above four-compartment assembly at a cell voltage of 1.0 V on sequential addition of 0.6 M CH_3OH, 0.6 M HCOOH and 0.6 M HCHO to the anodic chamber. **d**, Chronopotentiometry curves at a constant current of 10 mA from the same four-compartment assembly with or without 0.6 M HCHO in the anodic chamber and from the three-compartment assembly with no HCHO in the anodic chamber. **e**, Variation in the yield and FE of succinic acid production with consumed charge using the same four-compartment assembly. The purple and blue circles represent data for succinic acid in the chemical cells next to the cathodic and anodic chambers of the electrochemical cell, respectively. **f**, Variation in the yield and FE of succinic acid (SA) production with consumed charge using the above four-compartment assembly with or without 0.6 M HCHO and the three-compartment assembly. In **e** and **f**, the filled circles correspond to the results obtained after stirring for an extra 2 h after the electrolysis had ceased, and the red dashed arrows indicate the increase of the results obtained at the cease of electrolysis to those after an extra 2 h stirring. **g**, Variation in the amount of succinic acid produced with consumed charge during electrolysis using the above four-compartment assembly at applied currents of 10, 20 and 50 mA. **h**, Final total FEs for succinic acid obtained after electrolysis at 10, 20 and 50 mA. The error bars indicate the standard deviations of FE from measurements performed in triplicate.

new β-PdH_x phase was formed after the absorption of hydrogen atoms during the cathodic HER with a lattice parameter of 4.049 Å, an increase of 4.0% relative to the pristine Pd foil[35]. A nearly identical powder XRD pattern was obtained for the Pd foil after acting as the anode for the partial oxidation of HCHO (Fig. 2f). In addition, the Pd surface became rougher after serving as either cathode or anode (Supplementary Fig. 6). These results unambiguously prove that hydrogen absorption into the bulk Pd indeed occurred and that the Pd anode could form the same β-PdH_x phase during electrocatalytic HCHO oxidation. Thus, there is a great chance that the absorbed hydrogen might diffuse through the Pd membrane anode to the opposite side where hydrogen recombination to release H_2 (HER) may take place.

To increase the number of active sites for the HER, Pd was electrodeposited on the side of the Pd membrane anode facing the outside chamber, resulting in a Pd_{NP}/Pd membrane (see the Methods for details)[19]. XRD analysis confirmed that this new Pd_{NP}/Pd membrane electrode retained the same fcc phase structure as pristine Pd (Fig. 2f), although its (111) crystalline facet at 40.1° was more pronounced. Scanning electron microscopy (SEM) was conducted on the side of the Pd_{NP}/Pd membrane covered by electrodeposits and revealed a uniform coverage of the Pd surface by porous Pd nanoparticles and nanosheets (Supplementary Fig. 7). Accordingly, Pd_{NP}/Pd achieved an ~80-fold increase (Supplementary Fig. 8) in electrochemical double-layer capacitance (11.0 mF cm^{-2}) compared with the pristine Pd membrane electrode

https://doi.org/10.1038/s41929-023-00923-6

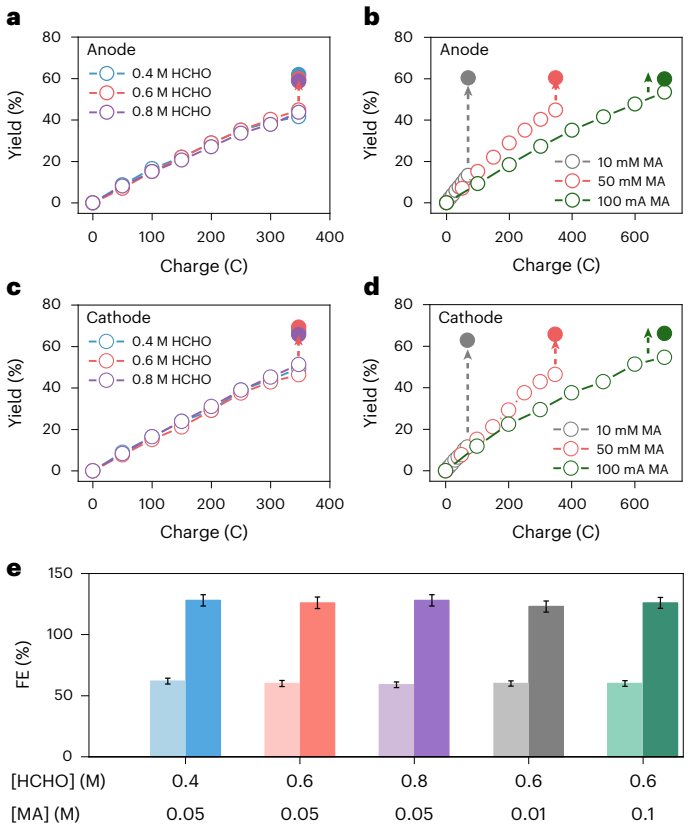

Fig. 4 | Electrocatalytic dual hydrogenation under various conditions. a,**c**, Variation in the yield of succinic acid produced in the chemical chamber next to the anode (**a**) and cathode (**c**) as the charge passed through the anode increases. The electrolysis experiments were performed with 0.4, 0.6 or 0.8 M HCHO in the anolyte at an applied current of 50 mA. **b**,**d**, Variation in the yield of succinic acid produced in the chemical chamber next to the anode (**b**) and cathode (**d**) as the charge passed through the anode increases. The electrolysis experiments were performed with 10, 50 or 100 mM maleic acid (MA) in the chemical chambers at an applied current of 50 mA. In **a**–**d**, the filled circles correspond to the yields obtained after stirring for an extra 2 h after the electrolysis had ceased, and the dashed arrows in indicate the increase of the results obtained at the cease of electrolysis to those after an extra 2 h stirring. **e**, Anodic FE (light shading) and total FE (dark shading) of the electrocatalytic hydrogenation of maleic acid at an applied current of 50 mA with varying HCHO and MA concentrations. The error bars indicate the standard deviations of FE from measurements performed in triplicate.

(0.134 mF cm^{-2}). To test the hypothesis that the Pd membrane anode can provide an escape route for the absorbed hydrogen generated from HCHO oxidation, chronopotentiometry experiments were conducted at currents of 20, 50 and 100 mA using the cell design shown in Fig. 2e and the H_2 produced was quantified (Fig. 2g). The amounts of H_2 generated in both the anodic chamber and the adjacent chemical chamber were recorded separately. In all cases, H_2 was detected as the sole gaseous product (Supplementary Fig. 9) and the amount of H_2 produced in the chemical chamber was far greater than that produced in the anodic chamber (Supplementary Fig. 10). Depending on the applied current, the total FE of H_2 generation on a Pd membrane anode ranged from 92% (20 mA) to 60% (100 mA), substantially higher than the values obtained from a Pd foil anode fully immersed in the electrolyte. These results unambiguously prove that the Pd membrane anode indeed provides an escape route for absorbed hydrogen to migrate to the opposite side. The effect of potential on anodic H_2 production was also investigated by applying different potentials (0.6, 0.8 and 1.0 V versus RHE) using our default anolyte (0.6 M HCHO in 1.0 M KOH) with a Pd membrane anode. The amounts of H_2 generated and FEs are plotted in Supplementary Fig. 11; the data show that for a higher potential, a smaller amount of H_2 was produced, accompanied by a lower FE, which is likely due to the greater contribution of the HOR at higher applied potentials.

Electrocatalytic dual hydrogenation of maleic acid

The above results gave us the confidence to explore electrocatalytic dual hydrogenation using our four-chamber assembly—an H-type electrochemical cell connected to two hydrogenation chambers on each side by a Pd membrane electrode. Figure 3a shows a photograph of our home-built reactor prepared in accord with this new design. The hydrogenation of maleic acid to succinic acid was selected as a model reaction as succinic acid is an important building block for polymers, solvents, fuel additives and pharmaceuticals, and is also among the US Department of Energy's Top 10 list of value-added platform molecules[36]. Using our four-compartment assembly (Fig. 3a) with 1.0 M KOH as the catholyte and a mixture of 1.0 M KOH and 0.6 M HCHO as the anolyte, the two Pd_{NP}/Pd membrane electrodes in a two-electrode configuration showed a rapid anodic current rise at ~0.4 V and a current density of over 15 mA cm^{-2} for a voltage input of 1.0 V by linear sweep voltammetry (Fig. 3b). In contrast, in the absence of HCHO, more than 2.5 V was required to reach the same current density using the same Pd_{NP}/Pd membrane electrodes for water splitting. If a competent OER electrocatalyst such as nickel foam was used in place of the Pd membrane anode, more than 2.0 V was still required to deliver a current density of 15 mA cm^{-2} (Fig. 3b) using a three-compartment assembly (Supplementary Fig. 12). As commercial HCHO solutions contain methanol as a stabilizer and its partial oxidation product formate can also be oxidized, it was of critical importance to assess the selectivity of the Pd membrane anode towards HCHO oxidation. As shown in Fig. 3c, the sequential addition of 0.6 M methanol and 0.6 M formic acid resulted in a negligible current increase at a cell voltage of 1.0 V, whereas the addition of 0.6 M HCHO led to an immediate anodic current rise. These results prove that the Pd membrane anode possesses excellent selectivity for the electrochemical oxidation of HCHO with low voltage input, which is not affected by the presence of either methanol or formate.

Next, chronopotentiometry was carried out with 50 mM maleic acid in the hydrogenation chambers on both sides of the four-compartment assembly. Compared with one-side hydrogenation coupled with water oxidation on a Pd_{NP}/Pd membrane or nickel foam anode at the same current of 10 mA, our electrocatalytic dual hydrogenation strategy saved around 1.7 or 1.0 V voltage input, respectively, to reach the same current (Fig. 3d). Quantification of the succinic acid produced in the hydrogenation chamber connected to the Pd_{NP}/Pd cathode showed a nearly linear increase in concentration with charge consumed (Fig. 3e; see the Supplementary Information for quantification details). At the end of the electrolysis, an 88% yield of succinic acid was achieved (Supplementary Fig. 13). Further stirring the hydrogenation solution for an additional 2 h resulted in an increased yield of 95%. This suggests that any absorbed hydrogen remaining in the Pd_{NP}/Pd cathode after electrolysis can continue to diffuse out of the cathode to drive the hydrogenation of maleic acid. Accordingly, the calculated FE also increased from 88% to almost 100%, highlighting the preference for hydrogenation over the HER. As expected, a similar amount of succinic acid was produced in the hydrogenation chamber connected to the Pd_{NP}/Pd membrane anode (Fig. 3e and Supplementary Fig. 14), corroborating our original hypothesis that hydrogen absorbed in a Pd membrane anode would also diffuse from the electrochemical side to the opposite side and undergo hydrogenation reactions. Furthermore, stirring for an additional 2 h after ceasing the electrolysis led to a slight increase in the succinic acid yield and FE. Overall, this electrocatalytic dual hydrogenation strategy not only saved substantial voltage input (Fig. 3d), but also doubled the succinic acid yield and total FE (total FE = 184%) compared with the one-side hydrogenation (FE = 90%) coupled with water oxidation on a Pd_{NP}/Pd membrane or nickel foam

https://doi.org/10.1038/s41929-023-00923-6

a

Substrate	Concentration (mM)	H source	Current (mA)	$Yield_A$ (%)	$Yield_C$ (%)	FE_S (%)
	50	HCHO	10	89	95	184
	50	HCHO	20	82	95	177
	50	HCHO	50	60	66	126
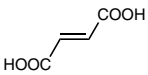	20	HCHO	10	66	64	130
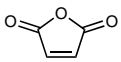	50	HCHO	10	87	97	184
	50	PFA	10	89	91	180

b

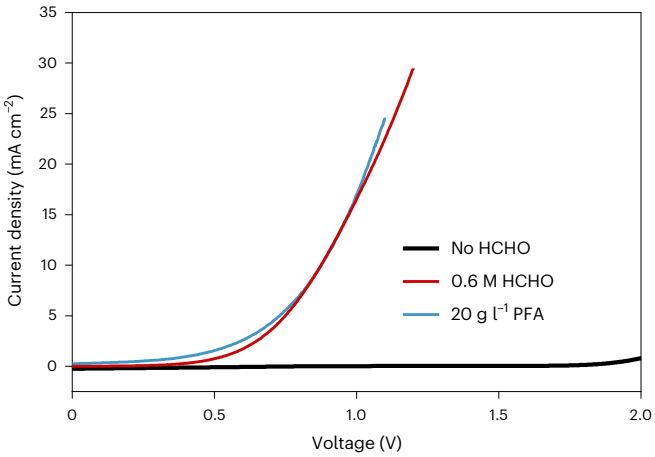

c

Fig. 5 | Versatility of electrocatalytic dual hydrogenation. a, Production of succinic acid from different biomass-derived unsaturated dicarboxylic acids. $Yield_A$, yield on anode side; $Yield_C$, yield on cathode side. **b**, LSVs of water splitting and the HER coupled with FOR using 0.6 M HCHO or 20 g l^{-1} PFA in the four-compartment assembly. **c**, Photograph of the succinic acid synthesized by the hydrogenation of 300 mM maleic anhydride.

anode (Fig. 3f and Supplementary Figs. 15 and 16) after passing the same amount of charge. Variation of the applied current (10, 20 and 50 mA) in the chronopotentiometry experiments revealed that more charge was required to realize the full conversion of maleic acid to succinic acid at 50 mA (Fig. 3g), and the corresponding total FE decreased from 184% at 10 mA to 177% and 126% at 20 and 50 mA, respectively (Fig. 3h and Supplementary Figs. 17–22), likely because the HER becomes more competitive at higher rates of H* formation. Finally, the organic species produced in the anolyte during HCHO oxidation were quantified and a carbon balance of nearly 100% was confirmed (Supplementary Figs. 23–29). Besides the products of the Cannizzaro reaction, additional formate was produced from the electrocatalytic oxidation of HCHO with an FE close to 100%, suggesting that the HOR was negligible under these conditions.

The decreasing FE of hydrogenation with increasing applied current prompted us to perform electrolysis experiments in which the concentrations of HCHO in the anolyte and maleic acid in the chemical chamber were varied. As shown in Fig. 4a, when the concentration of HCHO in the anolyte was increased from 0.4 to 0.8 M, there was no appreciable difference in the production rate and yield of succinic acid (Supplementary Figs. 30 and 31) when the electrolysis was carried out at 50 mA. In contrast, when the maleic acid concentration in the chemical chamber was reduced to 10 mM, after passing the theoretical amount of charge, the yield of succinic acid was only 13%, which was much lower than the yields obtained with higher concentrations (45% and 53% for 50 and 100 mM maleic acid, respectively; Fig. 4b and Supplementary Figs. 32 and 33). However, simply continuing to stir the hydrogenation solution for an extra 2 h after ending the electrolysis led to an increase in the yield of succinic acid to nearly 60% in all cases. Similar phenomena were observed for hydrogenation on the Pd membrane cathode (Fig. 4c,d and Supplementary Figs. 34–37). Finally, the anodic and total FEs remained nearly constant when different concentrations of HCHO and maleic acid were used (Fig. 4e). These results collectively indicate that when the electrolysis was performed at a higher current (50 mA compared with 10 mA), not all the rapidly generated H* migrated to the opposite side of the membrane for the hydrogenation of maleic acid and the competing HER was likely to occur.

Electrocatalytic dual hydrogenation of maleic acid analogues

Besides maleic acid, other important biomass-derived platform molecules, such as fumaric acid and maleic anhydride, can also be used as feedstock to produce succinic acid using our electrocatalytic dual hydrogenation strategy (Fig. 5a). Fumaric acid, the *E* isomer of maleic acid, gave a lower total FE of 130% (Supplementary Fig. 38), likely due

https://doi.org/10.1038/s41929-023-00923-6

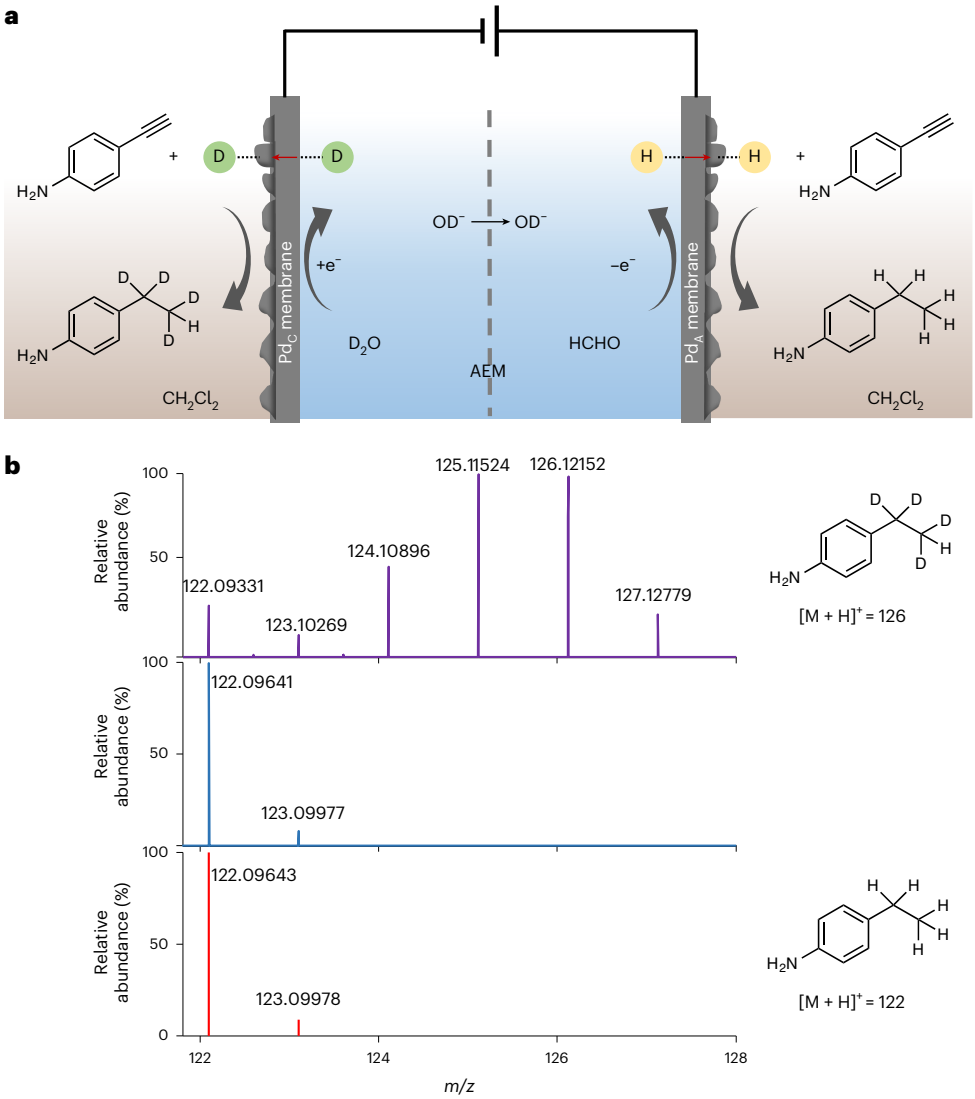

Fig. 6 | Investigation of the hydrogen source. a, Schematic of cathodic deuteration coupled with anodic hydrogenation of 4-ethynylaniline in a non-protic solvent (CH_2Cl_2). **b**, High-resolution mass spectra of the products (shown on the right) obtained from the electrolysis of 4-ethynylaniline in the chemical chambers next to the cathodic (purple) and anodic (blue) chambers, with the theoretical mass spectrum of $[C_8H_{11}N + H]^+$ (red) presented for comparison.

to the steric hindrance of its *trans* configuration. In contrast, excellent hydrogenation was achieved with maleic anhydride (total FE = 184%) because of its ready hydrolysis to maleic acid in aqueous media (Supplementary Fig. 39)[37]. In fact, the industrial production of succinic acid is currently dominated by the liquid-phase hydrogenation of maleic anhydride, which is typically performed in the temperature range of 120–180 °C at a H_2 pressure of 5–40 atm (ref. [38]). Compared with the liquid-phase and volatile HCHO stabilized by methanol, paraformaldehyde (PFA) is a cheaper, stable and solid-phase alternative that can be depolymerized to HCHO in aqueous media. Thus, PFA can also be used for hydrogen production[39,40]. Hence, we further explored the low-potential oxidation of PFA on a Pd foil anode in a three-electrode configuration (Supplementary Fig. 40a); a study of loading amount indicated that 20 g l^{-1} PFA in 1.0 M KOH gave the highest anodic current density of 44 mA cm^{-2} at 0.5 V versus RHE (Supplementary Fig. 40b). When the four-compartment assembly (Fig. 3a) was charged with anolyte containing 20 g l^{-1} PFA, our Pd_{NP}/Pd membrane electrode couple exhibited a nearly identical LSV curve to that collected with 0.6 M HCHO (Fig. 5b). Subsequent chronopotentiometry experiments using 20 g l^{-1} PFA in the anolyte with 50 mM maleic anhydride in both hydrogenation chambers also gave high yields of succinic acid with a total FE of 180% (Fig. 5a and Supplementary Fig. 41). Moreover, gram-scale production of succinic acid could be readily achieved by increasing the starting concentration of maleic anhydride. For instance, 300 mM maleic anhydride resulted in 2.4 g succinic acid isolated with high purity (Fig. 5c and Supplementary Fig. 42). Given the convenient decoration of Pd membrane electrodes by various hydrogenation catalysts[41], our reported strategy bears great promise for many organic hydrogenation reactions and large-scale applications.

Hydrogen source in electrocatalytic dual hydrogenation

To examine the versatility of our strategy and also determine the hydrogen source for hydrogenation on each side of the four-compartment assembly, 4-ethynylaniline, which is soluble in non-protic solvents, was investigated as a model substrate. In these experiments, 1.0 M KOD in D_2O was used as the supporting electrolyte with 20 g l^{-1} PFA in the anolyte. As schematically shown in Fig. 6a, it was expected that the deuterated product would be obtained on the cathode side, while

the normal hydrogenation product would be formed on the anode side. Indeed, chronopotentiometry at 50 mA using the same Pd_{NP}/Pd membrane electrodes resulted in deuterated and normal 4-ethylaniline on the cathode and anode sides, respectively, as confirmed by mass spectrometry (Fig. 6b and Supplementary Figs. 43 and 44) and ^{1}H NMR spectroscopy (Supplementary Fig. 45). These results prove that the hydrogen source for hydrogenation on the cathode side is water, while on the anode side it is PFA (that is, HCHO).

Conclusion

In summary, we have demonstrated that the low-potential oxidation of formaldehyde on a Pd membrane anode can produce active hydrogen atoms that are able to permeate through the membrane electrode to the opposite side for hydrogenation reactions. When two Pd membrane electrodes are employed, our electrocatalytic dual hydrogenation strategy enables the simultaneous hydrogenation of the same organic substrate in chambers outside of the electrochemical cell. The hydrogen sources for hydrogenation on the cathode and anode are water and formaldehyde, respectively. Compared with conventional one-side electrocatalytic hydrogenation, our dual hydrogenation strategy can save at least 1 V voltage input and double the hydrogenation rate and FE. Following this design, succinic acid can be successfully produced from biomass-derived maleic acid, fumaric acid, or maleic anhydride. Given the convenience of co-catalyst decoration of Pd membrane electrodes, we anticipate that this electrocatalytic dual hydrogenation strategy will be applicable to many organic hydrogenation reactions, with great potential for large-scale applications.

Methods

Electrochemistry

All electrochemical measurements were conducted on a VMP-3 potentiostat (Biologic Science Instruments). All reported potentials are referenced to the RHE by calibration using Pt as the working electrode in H_2-saturated 1.0 M KOH.

For the electrocatalytic oxidation of formaldehyde on Pd, a two-compartment electrochemical cell separated by an anion exchange membrane was used with Pd foil, Pt mesh and Hg/HgO (1.0 M KOH) as the working, counter and reference electrodes, respectively. The Pd foil working electrode and Hg/HgO (1.0 M KOH) reference electrode were placed in the anodic chamber, while the Pt mesh counter electrode was placed in the cathodic chamber. All linear sweep voltammetry experiments were conducted using a three-electrode configuration at a scan rate of 10 mV s^{-1} without *iR* correction.

To determine the electrochemical double-layer capacitance (C_{dl}), cyclic voltammograms were collected over a narrow range (±60 mV) centred around the open circuit potential (OCP) of each working electrode of interest at scan rates varying from 10 to 80 mV s^{-1}. The C_{dl} values were then estimated by plotting the difference (j) between the anodic (j_a) and cathodic (j_c) current densities ($j = j_a - j_c$) at the OCP versus the scan rate. The resulting linear slopes are equivalent to $2C_{dl}$.

Catalyst preparation

Pd_{NP}/Pd membrane electrodes were prepared by an electrodeposition method using 15.9 mM $PdCl_2$ and 1.0 M HCl as the electrolyte. Specifically, a Pd membrane, as the working electrode, was clamped between an electrochemical chamber and a chemical chamber, and a Pt mesh and a Ag/AgCl (saturated KCl) electrode were used as the counter and reference electrodes, respectively, in the electrochemical chamber. Electrodeposition was performed at a constant potential of −0.2 V versus Ag/AgCl until 16.75 C was passed.

Electrocatalytic dual H_2 production

For electrocatalytic dual H_2 production, a two-compartment electrochemical cell separated by an anion exchange membrane was used with two Pd foils as the anode and cathode, respectively. The electrolyte in the cathodic chamber was 1.0 M KOH(aq) (40 ml), while the anodic chamber contained 0.6 M HCHO in 1.0 M KOH (50 ml). Chronopotentiometry experiments were conducted at 20, 50 and 100 mA.

For electrocatalytic H_2 production on a Pd_{NP}/Pd membrane anode, a three-compartment assembly (Fig. 2e) was used with a Pd_{NP}/Pd membrane (area: 2.27 cm^2) and a Pd foil (area: 2 cm^2) as anode and cathode, respectively. The Pd nanoparticle side of the Pd_{NP}/Pd membrane faced the chemical chamber. The electrolyte in the cathodic chamber was 1.0 M KOH(aq) (40 ml), while the anodic chamber contained 0.6 M HCHO in 1.0 M KOH (50 ml); 40 ml water was added to the chemical chamber. Chronopotentiometry experiments were conducted at 20, 50 and 100 mA.

Electrocatalytic dual hydrogenation

For the electrocatalytic hydrogenation of maleic acid, a four-compartment assembly (Fig. 3a) was used with two Pd_{NP}/Pd membrane electrodes (area: 2.27 cm^2) as the cathode and anode, respectively. The Pd nanoparticle side of each Pd_{NP}/Pd membrane faced the chemical chamber for the hydrogenation reactions. The electrolyte in the cathodic chamber was 1.0 M KOH(aq) (40 ml), while the anodic chamber contained 0.6 M HCHO in 1.0 M KOH (50 ml); 50 mM maleic acid in water (36 ml) was added to the hydrogenation chambers on both sides of the electrochemical cell. LSVs were collected at a scan rate of 10 mV s^{-1} with 90% *iR* correction, while chronoamperometry experiments were performed at 10, 20 and 50 mA. The final product was obtained as a white solid after the evaporation of water. For comparison, a Ni foam (1 cm × 2.27 cm) was also used as the anode for water oxidation in the absence of HCHO in the anodic chamber, with a Pd_{NP}/Pd membrane electrode as the cathode for one-side hydrogenation of maleic acid.

Similar conditions were used for the electrocatalytic hydrogenation of fumaric acid. The only difference was that the concentration of fumaric acid was 20 mM. Chronopotentiometry experiments were carried out at 10 mA.

Similar conditions were also used for the electrocatalytic hydrogenation of maleic anhydride. In this case, 0.6 M HCHO or 20.0 g l^{-1} PFA was used in the anodic chamber. Chronopotentiometry experiments were carried out at 10 mA. For the large-scale electrolysis experiment, the concentration of maleic anhydride was 0.3 M. Chronopotentiometry experiments were carried out at 20 mA until 1.5-fold of the theoretical amount of charge for the complete conversion of maleic anhydride to succinic acid was passed.

Isotope experiment

The same four-compartment assembly was used for cathodic deuteration coupled with anodic hydrogenation of 4-ethynylaniline. The electrolyte in the cathodic chamber was 1.0 M KOD in D_2O (40 ml), while the anodic chamber contained 20.0 g l^{-1} PFA and 1.0 M KOD dissolved in D_2O (50 ml); 25 mM 4-ethynylaniline in dichloromethane (36 ml) was added to the hydrogenation chambers on both sides. Chronopotentiometry experiments were carried out at 50 mA.

Data availability

The data that support the findings of this study are included in the published article and the Supplementary Information. Further queries about the data can be directed to the corresponding author. Source data are provided with this paper.

References

1. Augustine, R. L. *Catalytic Hydrogenation: Techniques and Applications in Organic Synthesis* (Marcel Dekker, 1965).
2. Zhang, L., Zhou, M., Wang, A. & Zhang, T. Selective hydrogenation over supported metal catalysts: from nanoparticles to single atoms. *Chem. Rev.* **120**, 683–733 (2020).
3. Jagadeesh, R. V. et al. Nanoscale Fe_2O_3-based catalysts for selective hydrogenation of nitroarenes to anilines. *Science* **342**, 1073–1076 (2013).

4. Cui, X. et al. Highly selective hydrogenation of arenes using nanostructured ruthenium catalysts modified with a carbon–nitrogen matrix. *Nat. Commun.* **7**, 11326 (2016).
5. Friedfeld, M. R., Zhong, H., Ruck, R. T., Shevlin, M. & Chirik, P. J. Cobalt-catalyzed asymmetric hydrogenation of enamides enabled by single-electron reduction. *Science* **360**, 888–893 (2018).
6. Mas-Rosello, J., Smejkal, T. & Cramer, N. Iridium-catalyzed acid-assisted asymmetric hydrogenation of oximes to hydroxylamines. *Science* **368**, 1098–1102 (2020).
7. Lee, S. et al. Dynamic metal–polymer interaction for the design of chemoselective and long-lived hydrogenation catalysts. *Sci. Adv.* **6**, eabb7369 (2020).
8. Bondue, C. J., Calle-Vallejo, F., Figueiredo, M. C. & Koper, M. T. M. Structural principles to steer the selectivity of the electrocatalytic reduction of aliphatic ketones on platinum. *Nat. Catal.* **2**, 243–250 (2019).
9. Akhade, S. A. et al. Electrocatalytic hydrogenation of biomass-derived organics: a review. *Chem. Rev.* **120**, 11370–11419 (2020).
10. Gnaim, S. et al. Cobalt-electrocatalytic HAT for functionalization of unsaturated C–C bonds. *Nature* **605**, 687–695 (2022).
11. Fokin, S. Z. Die Rolle der Metallhydride bei Reduktionsreaktionen und neue Daten zur Erklärung der Frage über die Zusammen-Setzung einiger Fette und Trane. *Z. Elektrochem. Angew. Phys. Chem.* **12**, 749–768 (1906).
12. Lessard, J. *Organic Electrochemistry* (eds Hammerich, O. & Speiser, B.) 1658–1664 (CRC, 2015).
13. Li, T., Cao, Y., He, J. & Berlinguette, C. P. Electrolytic CO_2 reduction in tandem with oxidative organic chemistry. *ACS Cent. Sci.* **3**, 778–783 (2017).
14. You, B. & Sun, Y. Innovative strategies for electrocatalytic water splitting. *Acc. Chem. Res.* **51**, 1571–1580 (2018).
15. Sbei, N., Hardwick, T. & Ahmed, N. Green chemistry: electrochemical organic transformations via paired electrolysis. *ACS Sustain. Chem. Eng.* **9**, 6148–6169 (2021).
16. Cardoso, D. S. P., Šljukić, B., Santos, D. M. F. & Sequeira, C. A. C. Organic electrosynthesis: from laboratorial practice to industrial applications. *Org. Process Res. Dev.* **21**, 1213–1226 (2017).
17. Inoue, H., Abe, T. & Iwakura, C. Successive hydrogenation of styrene at a palladium sheet electrode combined with electrochemical supply of hydrogen. *Chem. Commun*. 55–56 (1996).
18. Iwakura, C., Yoshida, Y. & Inoue, H. A new hydrogenation system of 4-methylstyrene using a palladinized palladium sheet electrode. *J. Electroanal. Chem.* **431**, 43–45 (1997).
19. Iwakura, C., Abe, T. & Inoue, H. A new successive system for hydrogenation of styrene using a two-compartment cell separated by a Pd sheet electrode. *J. Electrochem. Soc.* **143**, L71–L73 (1996).
20. Sherbo, R. S., Delima, R. S., Chiykowski, V. A., MacLeod, B. P. & Berlinguette, C. P. Complete electron economy by pairing electrolysis with hydrogenation. *Nat. Catal.* **1**, 501–507 (2018).
21. Delima, R. S., Sherbo, R. S., Dvorak, D. J., Kurimoto, A. & Berlinguette, C. P. Supported palladium membrane reactor architecture for electrocatalytic hydrogenation. *J. Mater. Chem. A* **7**, 26586–26595 (2019).
22. Devanathan, M. A. & Stachurski, Z. The absorption and diffusion of electrolytic hydrogen in palladium. *Proc. R. Soc. A* **270**, 90–102 (1962).
23. Zheng, J., Sheng, W., Zhuang, Z., Xu, B. & Yan, Y. Universal dependence of hydrogen oxidation and evolution reaction activity of platinum-group metals on pH and hydrogen binding energy. *Sci. Adv.* **2**, e1501602 (2016).
24. Van Den Meerakker, J. E. A. M. On the mechanism of electroless plating. I. Oxidation of formaldehyde at different electrode surfaces. *J. Appl. Electrochem.* **11**, 387–393 (1981).
25. Machida, K. & Enyo, M. Formaldehyde electro-oxidation on copper metal and copper-based amorphous alloys in alkaline media. *Bull. Chem. Soc. Jpn* **58**, 2043–2050 (1985).
26. Wang, T. et al. Combined anodic and cathodic hydrogen production from aldehyde oxidation and hydrogen evolution reaction. *Nat. Catal.* **5**, 66–73 (2022).
27. Trincado, M., Grützmacher, H. & Prechtl, M. H. G. CO_2-based hydrogen storage—hydrogen generation from formaldehyde/water. *Phys. Sci. Rev.* **3**, 20170013 (2018).
28. Wang, C. & Astruc, D. Recent developments of nanocatalyzed liquid-phase hydrogen generation. *Chem. Soc. Rev.* **50**, 3437–3484 (2021).
29. Beltowskabrzezinska, M. Electrochemical oxidation of formaldehyde on gold and silver. *Electrochim. Acta* **30**, 1193–1198 (1985).
30. Beltowskabrzezinska, M. & Heitbaum, J. On the anodic oxidation of formaldehyde on Pt, Au and Pt/Au-alloy electrodes in alkaline solution. *J. Electroanal. Chem.* **183**, 167–181 (1985).
31. Martin, R. J. The mechanism of the Cannizzaro reaction of formaldehyde. *Aust. J. Chem.* **7**, 335–347 (1954).
32. Fukai, Y. *The Metal–Hydrogen System: Basic Bulk Properties* (Springer, 2006).
33. Holland, T. J. B. & Redfern, S. A. T. Unit cell refinement from powder diffraction data: the use of regression diagnostics. *Mineral. Mag.* **61**, 65–77 (1997).
34. Maeland, A. & Flanagan, T. B. Lattice constants and thermodynamic parameters of the hydrogen–platinum–palladium and deuterium–platinum–palladium systems. *J. Phys. Chem.* **68**, 1419–1426 (1964).
35. Benck, J. D., Jackson, A., Young, D., Rettenwander, D. & Chiang, Y.-M. Producing high concentrations of hydrogen in palladium via electrochemical insertion from aqueous and solid electrolytes. *Chem. Mater.* **31**, 4234–4245 (2019).
36. Bozell, J. J. & Petersen, G. R. Technology development for the production of biobased products from biorefinery carbohydrates—the US Department of Energy's 'Top 10' revisited. *Green. Chem.* **12**, 539–554 (2010).
37. Wojcieszak, R. et al. Recent developments in maleic acid synthesis from bio-based chemicals. *Sustain. Chem. Process.* **3**, 9 (2015).
38. Pinazo, J. M., Domine, M. E., Parvulescu, V. & Petru, F. Sustainability metrics for succinic acid production: a comparison between biomass-based and petrochemical routes. *Catal. Today* **239**, 17–24 (2015).
39. Suenobu, T., Isaka, Y., Shibata, S. & Fukuzumi, S. Catalytic hydrogen production from paraformaldehyde and water using an organoiridium complex. *Chem. Commun.* **51**, 1670–1672 (2015).
40. Fetzer, M. N. A., Tavakoli, G., Klein, A. & Prechtl, M. H. G. Ruthenium-catalyzed *E*-selective partial hydrogenation of alkynes under transfer-hydrogenation conditions using paraformaldehyde as hydrogen source. *ChemCatChem* **13**, 1317–1325 (2021).
41. Kurimoto, A. et al. Physical separation of H_2 activation from hydrogenation chemistry reveals the specific role of secondary metal catalysts. *Angew. Chem. Int. Ed.* **60**, 11937–11942 (2021).

Acknowledgements

Y.S. acknowledges the financial support of the National Science Foundation (CHE-1914546 and CHE-2102220), the Herman Frasch Foundation (820-HF17), the Michelman Green, Clean and Sustainable Technology Research Innovation Program, and the University of Cincinnati.

Author contributions

Y.S. conceived the idea and supervised the project. G.H. and G.L. performed the experimental work and data analysis. G.H. and Y.S. wrote the manuscript.

Competing interests

Y.S. has filed a provisional patent application related to this manuscript (US patent provisional 63/440,044). All other authors declare no competing interests.

Additional information

Supplementary information The online version contains supplementary material available at https://doi.org/10.1038/s41929-023-00923-6.

Correspondence and requests for materials should be addressed to Yujie Sun.

Peer review information *Nature Catalysis* thanks Shuangyin Wang, Hongyuan Sheng and the other, anonymous, reviewer(s) for their contribution to the peer review of this work.